Thermal Performance of Loop Heat Pipes with Smooth and Rough Porous Copper Fiber Sintered Sheets

Weisong Ling [a], Wei Zhou [a] *, Wei Yu [a], Ruiliang Liu [a], K. S. Hui [b]

[a] *Department of Mechanical and Electrical Engineering, Xiamen University, Xiamen 361005, China*

[b] *School of Mathematics, Faculty of Science, University of East Anglia, Norwich NR4 7TJ, United Kingdom*

Abstract: Smooth and rough porous copper fiber sintered sheets, employed here as wicks for loop heat pipes for the first time, were fabricated using a low-temperature solid-phase sintering method. The capillary performance of both of these types of porous copper fiber sintered sheets were analyzed and discussed. The influence of the surface morphology, filling ratio, and working fluid on the thermal resistance, evaporator wall temperature, and start-up time of the loop heat pipes were investigated. The results showed that the capillary pumping amount of working fluid for both smooth and rough porous copper fiber sintered sheets initially increases rapidly, and then gradually attains a stable state. The curve of the capillary pumping amount of working fluid can be described as a function that increases exponentially over time. When rough porous copper fiber sintered sheets are used as wicks and deionized water is used as the working fluid, the capillary pumping amount is maximized. Compared to smooth porous copper fiber sintered sheets, loop heat pipes with rough porous copper fiber sintered sheets exhibit a shorter start-up time, lower thermal resistance, and lower evaporator wall temperature. For a filling ratio in the range of 15 % - 45 %, loop heat pipes with rough porous copper fiber sintered sheets and a 30 % filling ratio show lower thermal resistance and a lower evaporator wall temperature. Ultimately, the use of deionized water as the working fluid with a 30 % filling ratio enables loop heat pipes with rough porous copper fiber sintered sheets to be stably operated at a heat load of 200 W.

Keywords：Loop heat pipe; porous copper fiber sintered sheet; surface morphology; capillary pumping amount; thermal performance

---

*Corresponding author. Tel.: 86-592-2188698; Fax: 86-592-2186383

E-mail address: weizhou@xmu.edu.cn (Wei Zhou)

1 Introduction

A loop heat pipe (LHP) is a highly efficient heat-transfer device that was initially proposed by scientists from the former Soviet Union in 1972 [1]. An LHP typically includes an evaporator, a condenser, steam and liquid lines, and working fluid as its main components. Further, an LHP exhibits excellent heat transfer performance with a steam-liquid phase change and has been widely used in many applications. For example, LHP without using the wick structure have developed to solve the problem of the high temperature and low efficiency of solar cells [2]. In the nuclear power field, a LHP have been designed for nuclear reactor power systems[3]. Especially, a mechanical pumped LHP can be also used for the aerospace industries[4]. Because the steam and liquid are separated and transferred through different pipelines [5], a reduction in the heat transfer efficiency caused by the entrainment limit [6] can be prevented efficiently. Thus, many new types of LHPs with different liquid-steam separators have been developed to improve the thermal performance by the experimental testing [7] and theoretical analyses [8]. As one of the most important parts of an LHP, the porous wick provides a capillary pumping force to drive the circulation flow of working fluid [9]. However, the porous wick should possess a lower flow resistance and larger permeability to establish a flow channel for the liquid fluid [10].

The wick structure has a great influence on the capillary pumping performance of an LHP. In fact, many researchers have devoted considerable efforts to optimize and enhance the capillary performance of porous wicks [11]. Previous studies found that micro-groove wicks with simple structures are easy to fabricate [12]. However, the capillary force is insufficient because of the larger average size of these wicks and the limits in terms of their direction selectivity. Subsequently, multi-layer mesh wicks were developed to solve the problem of direction selectivity, but the capillary force remained insufficient for the increasing heat flux of electronic chips [13]. In recent years, many researchers have focused on sintered wicks. Sintered powder wicks, with effective three-dimensional network and fine pore structures, have been widely used in LHPs [14]. For example, Wu *et al.* [15] developed a novel sintered nickel powder wick for application in LHPs. The results showed that the thermal resistance of the LHP was as low as 0.095 °C/W, and the evaporator heat transfer coefficient was measured as 131 kW/ (m^2·K). Zhang *et al.* [16] investigated the effects of the sintering parameters on the porosity, pore size, permeability, and capillary pumping rate of wicks with nickel and nickel-copper powder, and the influence of the sintering time and temperature was also observed to be significant. Li *et al.* [17] developed two kinds of wick structures, i.e., single-powder (SP) and continuous step-graded (CSG) wicks, for LHPs. The heat transfer performance of the LHP with a continuous step-graded wick was found to be much higher than that of a single-powder wick.

The contradiction between the capillary pumping force and permeability of wicks has led to the development of innovative bi-porous wick structures [18]. These wicks usually possess two different pore sizes and intertexture each other. The smaller pore size provides the capillary force that drives the flow of the liquid working fluid, whereas the larger pore size establishes the flow channel for the liquid working fluid.

Chen *et al.* [19] fabricated a sintered nickel powder bi-porous wick for a plate-type evaporator in an LHP. The results showed that the LHP had a heat load of 130 W with an evaporator wall temperature of 60 °C, and a thermal resistance of 1.42 - 0.33 °C/W with a heat load of 10 - 130 W. Li *et al.* [20] proposed cold pressing sintering and loose powder sintering methods to fabricate nickel powder bi-porous wicks. The maximum porosity and permeability of these wicks could reach 77.4 % and 3.15×10^{-13} m^2, respectively. A previous study proposed the use of multi-layer metal foams and composite porous copper fiber sintered sheets as wick structures for LHPs. Improved heat transfer performance was observed for the LHPs with different heat loads [21-22].

Recently, many researchers carried out numerous research studies to investigate performance parameters such as the capillary pumping force of the wick in LHPs. Nishikawara *et al.* [23] studied the effect of introducing gaps between the wick and evaporator wall on the heat transfer performance using numerical simulation methods. The results showed that the optimum gap enhanced the heat transfer performance when a wick with a low thermal conductivity coefficient was selected. Liu *et al.* [24] developed two sintered nickel powder wicks embedded in the evaporator of LHPs. With a heat load range of 10 - 170 W, the LHPs could successfully start up with the evaporator wall temperature below 90 °C. Cheng *et al.* [25] investigated the capillary pumping performance of a porous wick in an LHP by developing a method that studied real-time changes in the curve of the capillary pumping amount. The results showed that the real-time changes in the curve of the capillary pumping amount recorded by an electronic balance and a computer could be described by an exponentially increasing equation.

Prior research focused on the structural designs, fabrication methods, and improvements in the heat transfer performance of the porous wicks in LHPs. The effects of the surface morphology on the thermal performance of LHPs have not been reported in the literature. In this study, both smooth and rough porous copper fiber sintered sheets (PCFSSs), which were employed as wicks, were fabricated using the low-temperature solid-phase sintering method for LHPs. The capillary pumping performance of smooth and rough PCFSSs was tested and analyzed. Furthermore, the influences of the surface morphology, filling ratio, and working fluid on the thermal resistance, evaporator wall temperature, and start-up time of LHPs were investigated in detail.

Nomenclature			
A	Area, m^2	Subscripts	
FR	Filling ratio, %	*amb*	Ambient
D	Diameter, m	*cap*	Capillary
H	Height, m	*cond*	Condenser
K	Permeability, m^2	*cro*	Cross-sectional
K'	Relative permeability, $m^2 \cdot s/kg$	*eva*	Evaporator
L	Length, m	*ec*	Evaporator and condenser
M	Capillary pumping amount, g	*ed*	Equivalent diameter
N	Number	*ep*	Equivalent diameter of pore
P	Pressure, Pa	*eff*	Effective
ΔP	Pressure difference, Pa	*l*	Liquid
Q	Heat load, W	*s*	Steam
Q_{FL}	Filled-liquid mass limit, kg	*s.line*	Steam line
R	Thermal resistance, ℃/W	*l.line*	Liquid line
S	Suppositional area, m^2	*w*	Wick
T	Temperature, ℃		
ΔT	Temperature difference, ℃		

V	Volume, m^3	CC	Compensation chamber
V_{FL}	Filled-liquid volume limit, m^3		
g	Gravitational acceleration, m/s^2	Greek symbols	
h	Heat transfer coefficient, W/ (m^2·K)		
h_{fg}	Latent heat, kJ/kg	μ	Dynamic viscosity, Pa·s
m	Quality, kg	ε	Porosity, %
q	Heat flux, W/m^2	ρ	Density, kg/m^3
r	Radius, m	τ	Time constant, s
x	Constant coefficient about wick	η	Kinematic viscosity， m^2/s
t	Time, s	σ	Surface tension, N/m
y_0	Maximum capillary pumping amount, g	θ	Contact angle, °
		φ	Fiber volume fraction, %
	Abbreviations		
SEM	Scanning electron microscope		
LHP	Loop heat pipe		
PCFSS	Porous copper fiber sintered sheets		

2 Experimental setup

After the introduction of fabrication process of rough and smooth copper fibers, the experimental test device for capillary pumping amount of rough and smooth PCFSSs was established. Subsequently, the structural design and testing system of LHP was described. Meanwhile, the important performance parameters such as capillary force, thermal resistance and heat transfer coefficient, and so on were determined for the LHP with PCFSS as wick. In the last, the uncertainty analysis for some parameters and devices was also provided.

2.1 Fabrication process of smooth and rough porous copper fiber sintered sheets

Compared to the copper powder sintered wicks, the porosity of copper fiber sintered wicks varied from 50% - 95% under controlled conditions, as calculated by Eq. (7). The copper fiber sintered wicks exhibited larger permeability of 10^{-8} m^2 to 10^{-10} m^2, as obtained by Eq. (8). The low-temperature solid-phase sintering method was employed to fabricate smooth and rough PCFSSs using copper fibers with both rough and smooth surface morphologies [26]. The copper fiber with a rough surface morphology and an equivalent diameter of 100 μm was fabricated by the cutting method using a multi-tooth tool [27], as shown in Fig. 1 a. Based on the scanning electron microscope (SEM) (SU-70, Hitachi, Japan) results, it was obvious that there were many microstructures distributed on the surface of the rough copper fiber. The smooth surface morphology copper fiber with an equivalent diameter of 100 μm was fabricated by the drawing method, as shown in Fig. 1 b. The SEM images of smooth and rough PCFSSs are shown in Fig. 1 c and d, respectively. The three-dimensional reticulated structure of the smooth and rough PCFSSs could easily be observed. The 3D surface topography of copper fiber with rough and smooth surfaces, as detected by Laser Scanning Microscope (VK-X200K, KEYENCE, Japan), is shown in Fig. 2, and the corresponding roughness values are shown in Fig. 3. The roughness (Ra) of the rough fiber was determined to be 27 times than that of the smooth fiber.

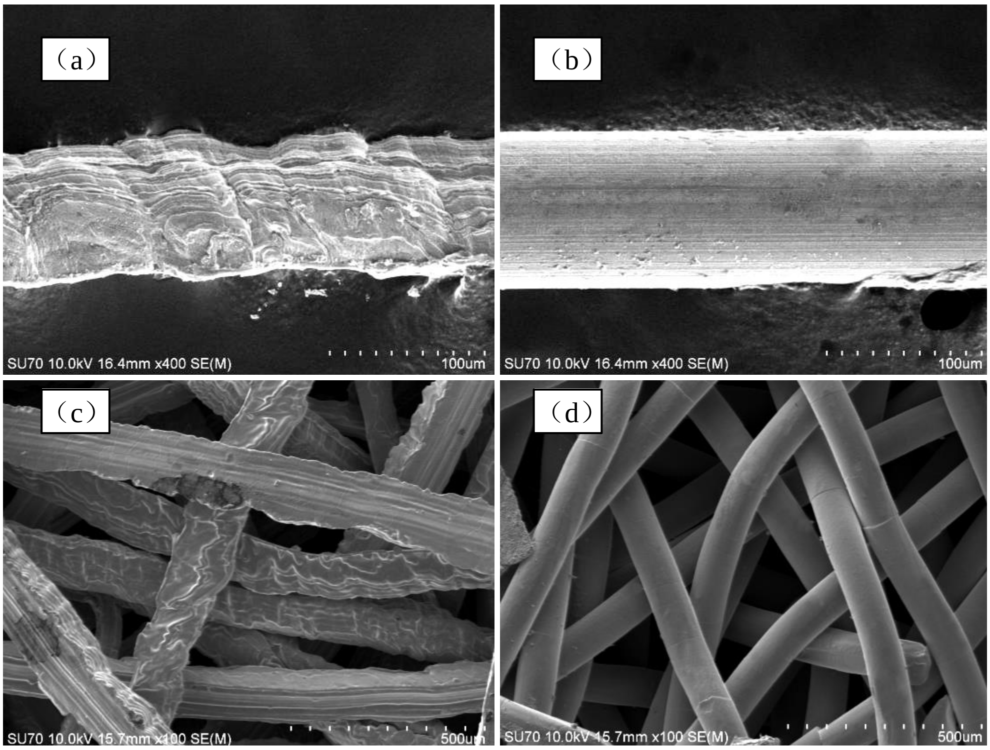

Fig. 1 SEM images of smooth and rough PCFSSs fabricated using low-temperature solid-phase sintering method

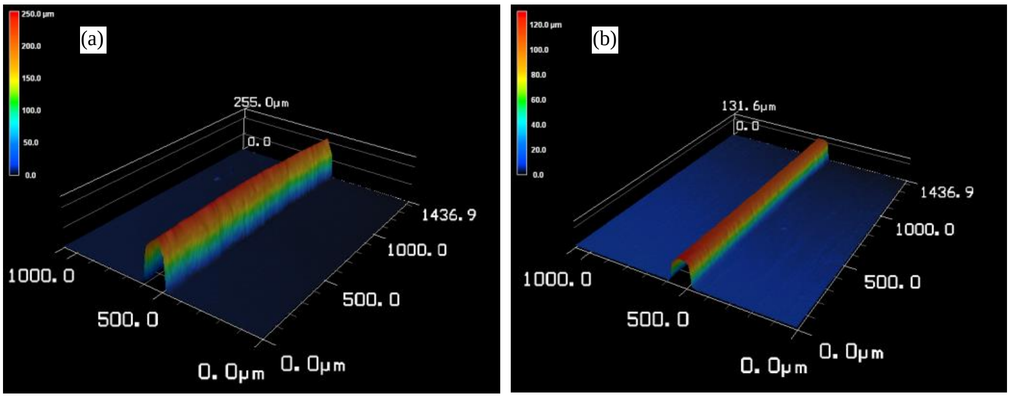

Fig. 2 3D surface topography of copper fiber by Laser Scanning Microscope:

(a) Rough copper fiber; (b) Smooth copper fiber

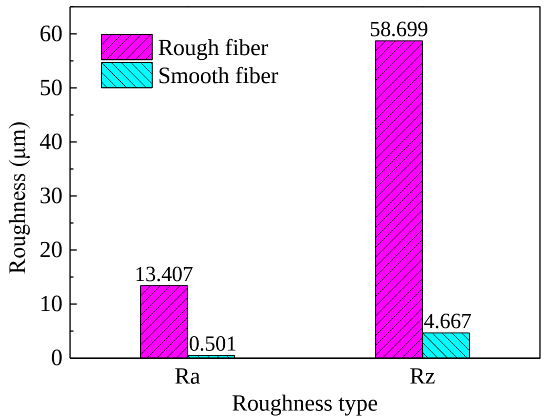

Fig. 3 Roughness of rough and smooth copper fiber

2.2 Capillary pumping performance test of porous copper fiber sintered sheets

The equipment used in the capillary pumping test device to assess the performance of the PCFSS included a high-precision electronic balance (precision of 0.0001 g, Sartorius, Germany), a mechanical elevator, a beaker, a computer, and liquid working fluid, as shown in Fig. 4. The accuracy of the measurement was ensured by covering the electronic balance with transparent glass to limit liquid evaporation and air fluctuations. The computer exchanged data with the electronic balance to provide a real-time display and record changes in the quantity of liquid working fluid. The mechanical elevator was used to control the upward and downward movements of the wick. Because of continuous evaporation of the working fluid, regardless of the presence of a wick sample therein, the data collected directly by the computer (M_{total}) contained the capillary pumping amount of the wick (M_{cap}) and the evaporation amount of working fluid (M_{eva}). A non-sample evaporation experiment was firstly conducted to obtain the evaporation amount of working fluid (M_{eva}), and then the required capillary pumping amount of the wick was calculated based on Eq. (1). During the measuring process, the electronic balance was set to zero, and then the beaker was filled with the appropriate amount of working fluid. By manipulating the mechanical elevator, the wick moved downward slowly. The data (M_{total}) was immediately recorded when the wick came into contact with the liquid surface. The wick was dipped into the liquid to a certain depth (about 3 mm) during the measuring process to prevent the level of the liquid from dropping. The ambient temperature was approximately 25 ± 1 °C.

$$M_{cap} = M_{total} - M_{eva} \tag{1}$$

where M_{cap} is the required capillary pumping amount of the wick, M_{total} is the total mass recorded by the computer, and M_{eva} is the evaporation amount of working fluid.

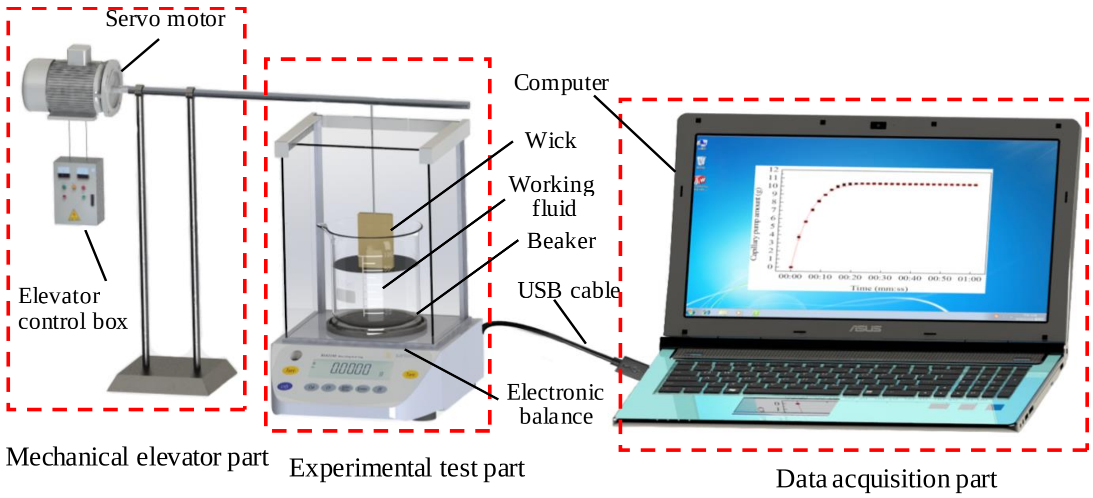

Fig. 4 Experiment schematic for measuring the capillary pumping amount of PCFSSs

2.3 Structural design and testing system of loop heat pipe

Fig. 5 shows the structural schematic of the developed LHP. The LHP consists of an evaporator with a porous wick and a compensation chamber and steam grooves, a condenser, steam-liquid lines, thermocouples and so on, as shown in Fig. 6. The detailed parameters of the designed LHP are listed in Table 1. In a previous study, the system that was used to test the LHPs comprised a data acquisition system, an auxiliary heating system, and an enhanced convection cooling system [22]. A total of 12 k-type thermocouples were used to measure the temperature at different locations in the LHP. The temperature of the steam and liquid were measured by installing four inserted thermocouples in direct contact with the working fluid at the inlet and outlet of the evaporator and condenser, respectively. The smooth and rough PCFSSs with a porosity of 70 % were applied to the evaporator. The gap between the wick and evaporator wall was sealed to prevent steam from infiltrating the compensation chamber. The thermophysical properties varied for different working fluids, as shown in Table 2. The capillary pumping performance and heat transfer performance were strongly influenced by thermophysical properties such as the latent heat, surface tension, and boiling point. In this study, deionized water, acetone, and ethanol were selected as working fluids with three filling ratios of 15 %, 30 %, and 45 %. The working fluids were sufficiently degassed to exclude the effect of non-condensable gases.

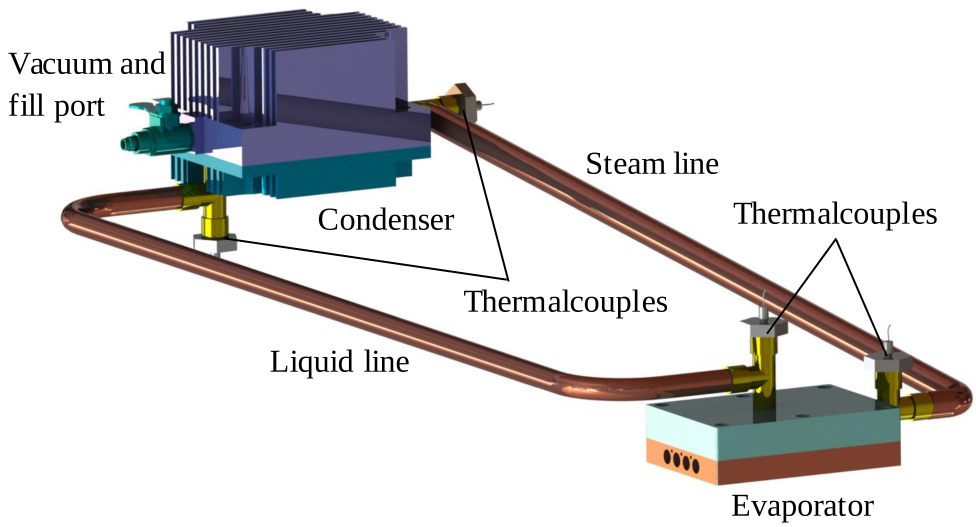

Fig. 5 Structural schematic of developed LHP

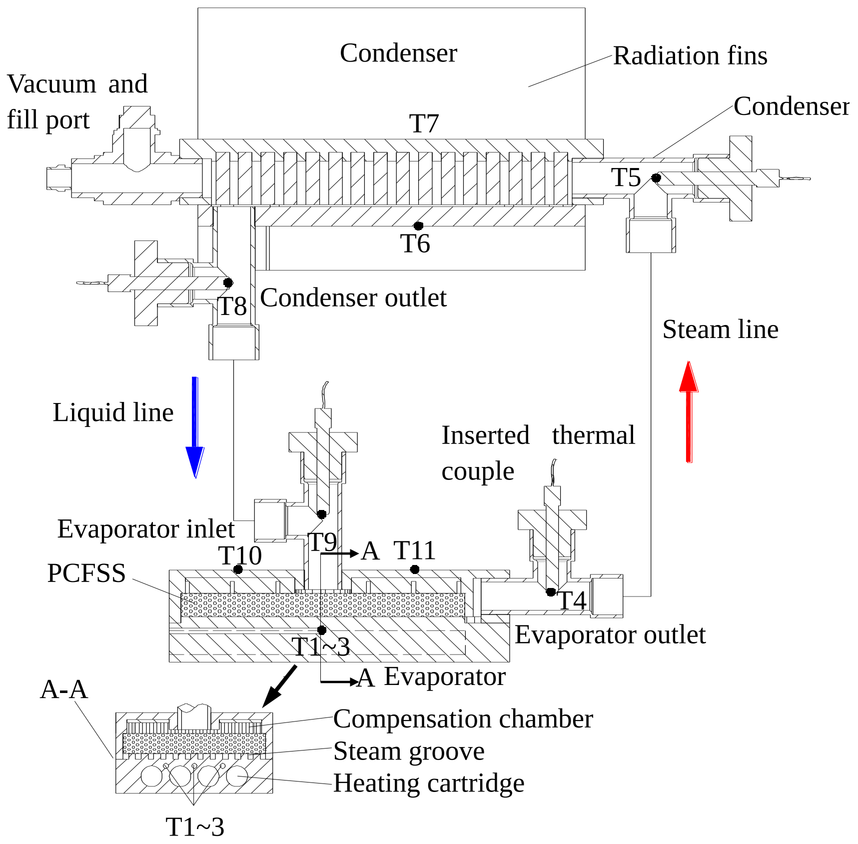

191

192 Fig. 6 Sectional view of developed LHP

193 Table 1 Dimension parameters of developed LHP and its components

Parameter	Material	Value	Unit
Evaporator	Aluminum alloy		
Length * width * height		78*44*13.5	mm^3
Steam groove	Pure copper		
Depth*width*spacing		1.5*1.5*2	mm^3
Condenser	Aluminum alloy		
Length * width * height		80*70*10.5	mm^3
Steam line	Pure copper		
Outer *inner diameter*length		8*5*200	mm^3
Liquid line	Pure copper		
Outer *inner diameter*length		6*4*200	mm^3
Porous wick	Copper fiber		
Length * width * height		70*40*6	mm^3
Porosity		70	%
Smooth fiber diameter		100	μm
Rough fiber diameter		100	μm

Heating block	Pure copper		
Length * width * height		78*44*8	mm^3
Cartridge	Stainless steel		
Diameter*length*number		6*73*4	mm^2
Total power		150*4	W

2.4 Date reduction

The capillary force is the main force driving the working fluid, and the flow is predominantly influenced by the effective pore size of the wick and surface tension of the liquid. The maximum capillary force is calculated according to the following equation:

$$(\Delta P_{cap})_{\max} = \frac{2\sigma}{(r_w)_{eff}} \cos\theta \qquad (2)$$

where $(\Delta P_{cap})_{\max}$ is the maximum capillary force, σ is the surface tension of the liquid, $(r_w)_{eff}$ is the effective pore radius of the wick, and θ is the contact angle between the liquid and the surface of the wick. Assuming that the contact angle is 90°, Eq. (2) can be simplified as follows:

$$(\Delta P_{cap})_{\max} = \frac{2\sigma}{(r_w)_{eff}} \qquad (3)$$

A pressure drop occurs when the working fluid flows through each part of the LHPs, and only when the capillary force generated by the wick is larger than the sum of the pressure drops can the wick become saturated and can working fluid circulation proceed. This relationship is described as follows [28]:

$$(\Delta P_{cap})_{\max} \geq \Delta P_s + \Delta P_l + \Delta P_w + \Delta P_{cond} - \Delta P_{axial} \qquad (4)$$

where ΔP_s, ΔP_l, ΔP_w, and ΔP_{cond} are the pressure drops in the steam and liquid lines, wick, and condenser, respectively. ΔP_{axial} is the static axial pressure drop, with the negative sign indicating that the condenser is located above the evaporator.

The thermal resistance (R_{LHP}) of LHPs was calculated via the following temperature difference equation [29]:

$$R_{LHP} = \frac{T_{eva} - T_{cond}}{Q} \quad (5)$$

where T_{eva} and T_{cond} are the average temperatures of the evaporator and condenser, respectively, and $T_{eva} = \frac{T1+T2+T3}{3}$, $T_{cond} = \frac{T6+T7}{2}$, and Q is the heat load.

The heat transfer coefficient of the LHP is calculated via the following equation:

$$h_{LHP} = \frac{Q}{A_{eva}(T_{eva} - T_{cond})} \quad (6)$$

where A_{eva} is the bottom surface area of the evaporator.

The porosity of a wick signifies the ratio of the pore volume to the volume of the entire wick, which is expressed as:

$$\varepsilon = \left(1 - \frac{m_{copper}}{\rho V_w}\right) \times 100\% \quad (7)$$

where ε is the porosity of the wick, m_{copper} is the quality of the copper fibers, ρ is the density of copper, and V_w is the volume of the wick. This method enables the porosity to be actively controlled within the range 50%-95%.

The permeability K is calculated as follows [30]:

$$K = \frac{r^2}{16\varphi^{3/2}\left(1+56\varphi^3\right)} \quad (8)$$

where r is the equivalent radius of the copper fiber, which is 50 μm in this study. Further, φ is the fiber volume fraction, which is defined as:

$$\varphi = 1 - \varepsilon \quad (9)$$

where ε is the porosity of the wick.

The relative permeability K' is defined as:

$$K' = \frac{K}{\mu L_w} \quad (10)$$

where μ is the dynamic viscosity of the working fluid and L_w is the length of the wick.

2.5 Uncertainty analysis

The uncertainties in individual temperature measurements are ±0.3 °C for the type-K thermocouples. The supply power measured by the wattmeter yields an uncertainty of 0.5 %. The uncertainties in the geometry dimension are estimated to be 0.5-1 %. The uncertainty in the electronic balance measurements is estimated at ±0.05 mg. The evaporator wall temperature and condenser temperature uncertainties stem from the thermocouple errors, and the uncertainty in the thermal resistance of the LHPs has its origins in the evaporator and condenser temperature errors and the supply power error, as shown in Eq. (5). The uncertainties associated with the measured and reduced parameters are obtained using a standard error analysis method [31]. The uncertainties in the evaporator wall temperature, condenser temperature, and thermal resistance are calculated as ± 0.52 °C, ± 0.42 °C, and ± 0.050 °C/W, respectively.

3 Results and discussion

The capillary pumping performance of PCFSSs were studied firstly, and then the theoretical value of capillary pumping amount and time constant were calculated based on Darcy’s law. Later, the influences of surface morphology, filling ratio, and working fluid on the thermal performance of LHPs with PCFSSs as wicks were also studied in detail. Finally, the stable operation test was conducted to investigate the thermal performance of LHP.

3.1 Capillary pumping test

As a typical phase-change heat transfer device, an LHP mainly transfers heat through evaporation and condensation of the working fluid. The heat transfer rate of the LHP depends on the transfer rate of the working fluid associated with the capillary pumping performance of the porous wicks. While the LHP was running, the working fluid in the wick constantly evaporated, and the wick absorbed the working fluid from the compensation chamber through the capillary pumping force. When the capillary pumping rate was larger than the evaporation rate, the wick was saturated with liquid. However, the saturation of the wick was reduced when the capillary pumping rate was less than the evaporation rate. To achieve a new balance for the LHP, the capillary pumping rate was increased and the evaporation rate was reduced. This resulted in fluctuation of the evaporator wall temperature [28].

According to Darcy's law [32]:

$$S(H(t)-H_0)=K^{'}A_{cro}\int_0^t \rho g[L_w-H(t)]dt \qquad (11)$$

where $H(t)$ is the real-time capillary pumping height, H_0 denotes the capillary pumping height when t = 0. K' is the relative permeability of the wick ($m^2 \cdot s/kg$) and $K'=K/(\mu L_w)$, where μ is the dynamic viscosity of the working fluid. A_{cro} is the cross-sectional area of the wick (m^2), S is the suppositional dense tube area when the quality and height were same with the wick (m^2), S/A_{cro} is the porosity ε of the wick, ρ is the density of the liquid working fluid (kg/m^3), and L_w is the length of the wick (m).

When t = 0, H (0) = H_0 = 0, then Eq. (11) can be rewritten as:

$$H(t)=\frac{K^{'}A_{cro}\rho g}{S}\int_0^t[L_w-H(t)]dt \quad (12)$$

By replacing $\varepsilon=S/A_{cro}$ into Eq. (12), it becomes

$$dH(t)=\frac{K^{'}\rho g}{\varepsilon}[L_w-H(t)] \quad (13)$$

Solving Eq. (13), it becomes

$$\ln[L_w-H(t)]=-\frac{K^{'}\rho g}{\varepsilon}t+C \quad (14)$$

When t = 0, H (0) = H_0 =0, C can be computed as:

$$C=\ln L_w \quad (15)$$

According to Eqs. (14) and (15), the capillary pumping height can be calculated as:

$$H(t)=L_w-e^{-\frac{K^{'}\rho g}{\varepsilon}t+C}=L_w(1-e^{-\frac{K^{'}\rho g}{\varepsilon}t}) \quad (16)$$

The capillary pumping height equation can be converted into a quantity equation as:

$$M(t)=\rho A_{cro}\varepsilon H(t)=\rho A_{cro}\varepsilon L_w(1-e^{-\frac{K^{'}\rho g}{\varepsilon}t}) \quad (17)$$

As was well known, the curve of capillary pumping amount of the wick was an exponential equation [25], and the classic capillary pumping amount was expressed as

$$y=y_0+A_0\cdot e^{-t/\tau} \quad (18)$$

where y_0 is the maximum capillary pumping amount, A_0 is the amplitude, τ is the time constant, which represented the time when the capillary pumping amount was 63.2% (1-1/e) of the maximum amount.

Fig. 7 shows the fitting curve of the capillary pumping amount action with deionized water as the working fluid and a rough PCFSS. It was obtained from the fitting curve that $y_0 = -A_0 = 10.5$ g, $\tau = 5.05$ s, and this indicated that the capillary pumping amount of rough PCFSS was large and the working fluid took a shorter time to reach a stable state. Comparing Eqs. (17) and (18), the maximum capillary pumping amount $y_0 = \rho A_{cro} \varepsilon L_w$ and the time constant $\tau = \varepsilon / (K' \rho g)$. Choosing deionized water as working fluid, the maximum capillary pumping amount could be calculated as $y_0 = 11.76$ g, $\tau = 4.61$ s, which agrees well with the experimental values of 10.5 g and 5.05 s.

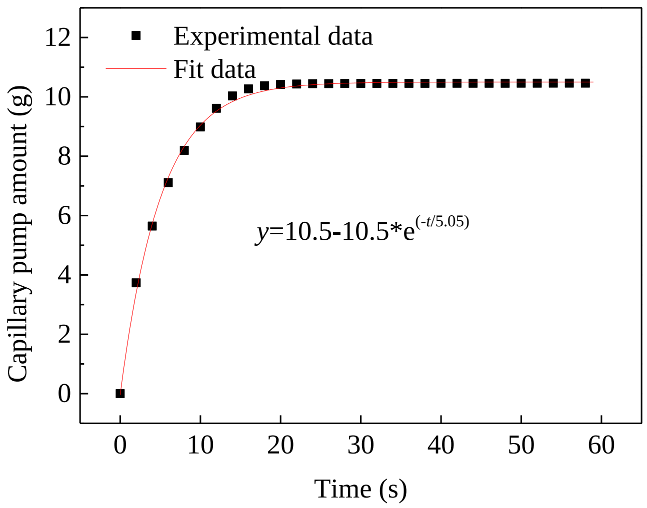

Fig.7 Capillary pump performance fitting curve

The curves of the capillary pumping amount with deionized water, acetone, and ethanol as working fluids for smooth and rough PCFSSs are shown in Fig. 8. For the three working fluids, it was found that the capillary pumping amount and the capillary pumping rate with rough PCFSSs were much larger than those of smooth PCFSSs. When acetone was used as the working fluid, the capillary pumping amount difference between the smooth and rough PCFSSs was 2.7056 g, which means that the capillary pumping amount of rough PCFSS was increased by 64% compared with smooth PCFSS. This was mainly attributed to the existence of many microstructures on the fiber surface of rough PCFSS, which provided a greater capillary pumping force and stored larger amounts of liquid [33].

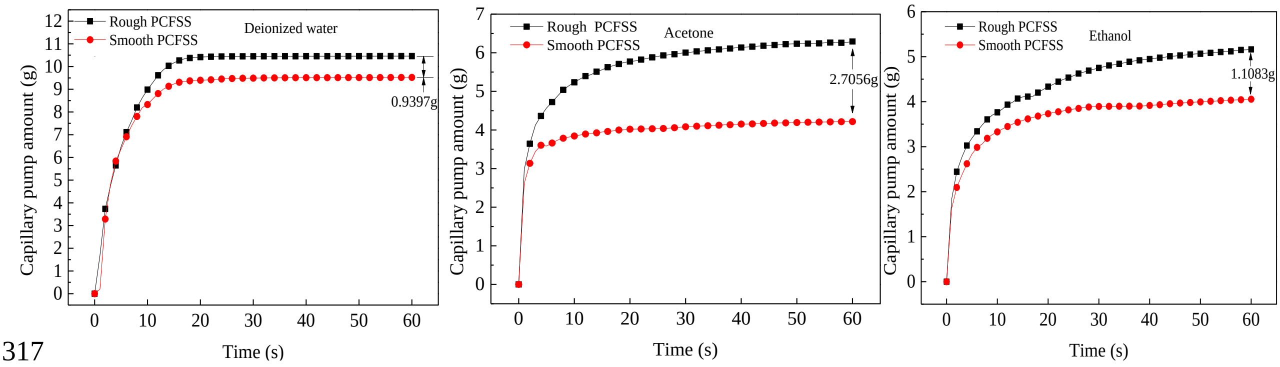

Fig. 8 Capillary pumping performance of rough and smooth PCFSSs wick under different working fluids: (a) deionized water; (b) acetone; (c) ethanol

The working fluids deionized water, acetone, and ethanol have different boiling points, densities, and surface tensions, as shown in Table 2. Fig. 9 compares the capillary pumping performance of rough PCFSSs for the three working fluids. Compared to ethanol and acetone, the largest capillary pumping amount i.e., approximately 10.4618 g, was measured for deionized water. This could be attributed to the following: rough PCFSSs absorbed a larger volume of deionized water owing to their larger surface tension. Meanwhile, because the density of deionized water is higher, the largest capillary pumping amount for rough PCFSS was obtained. According to Table 2, acetone and ethanol were observed to have a similar density at 25 °C. However, a much larger capillary pumping amount was obtained for acetone. This was mainly ascribed to the larger surface tension of acetone, and its good compatibility and wettability with copper fibers. Furthermore, it was found that the three working fluids required different amounts of time to attain a stable status. The shortest time of approximately 18 seconds was observed for deionized water. When the heat load was changed, the wick reached a new equilibrium between the capillary pumping rate and evaporation rate within a short period of time, thus causing a smaller temperature fluctuation in the LHP. The enlarged figure in Fig. 9 shows that acetone exhibited the highest capillary pumping rate in the initial capillary pumping stage owing to its excellent compatibility and wettability with rough PCFSS.

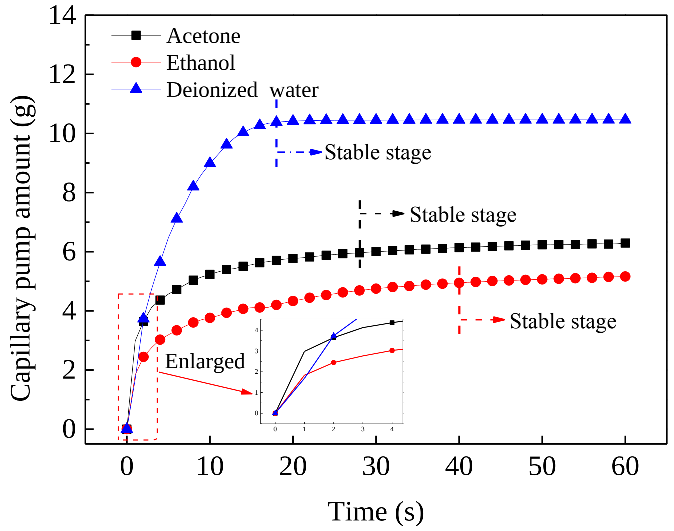

Fig. 9 Comparison of capillary pumping performance of rough PCFSSs with different working fluids

Table 2 Boiling point, density, and surface tension of different working fluids (25℃, 1.01x10^5 Pa)

Working fluids	Boiling point (℃)	Density (g/cm^3)	Surface tension (m·N/m)	Latent heat (kJ/kg)
Deionized water	100	1	71.99	2257.6
Acetone	56	0.788	24	524
Ethanol	78	0.785	21.8	812

3.2 Thermal performance test

In this study, the surface morphology, filling ratio, and working fluid were varied to study the thermal performance of LHPs including the evaporator wall temperature, thermal resistance, and start-up time.

3.2.1 Surface morphology

Fig. 10 shows the thermal performance of LHPs with smooth and rough PCFSSs under different heat loads when deionized water with a 30 % filling ratio was used as working fluid. It can be seen that the evaporator wall temperature, thermal resistance, and start-up time of LHPs with rough PCFSSs were lower than the smooth PCFSSs. This could be attributed to the following reasons: the microstructures on the surface of rough PCFSSs increased the specific surface area and heat exchange surface. This characteristic was beneficial to accelerate the evaporation of working fluid and heat transfer. On the other hand, the microstructures also provided a larger capillary pumping force and absorbed sufficient liquid working fluid to avert the dry-out phenomenon. A larger amount of heat was transferred to the condenser with rough PCFSS; hence, the temperature near the evaporator with rough PCFSS as the wick was lower than that with smooth PCFSS, and the temperature near the condenser was exactly the opposite when a 100 W heat load was selected, as shown in Fig. 10 (d).

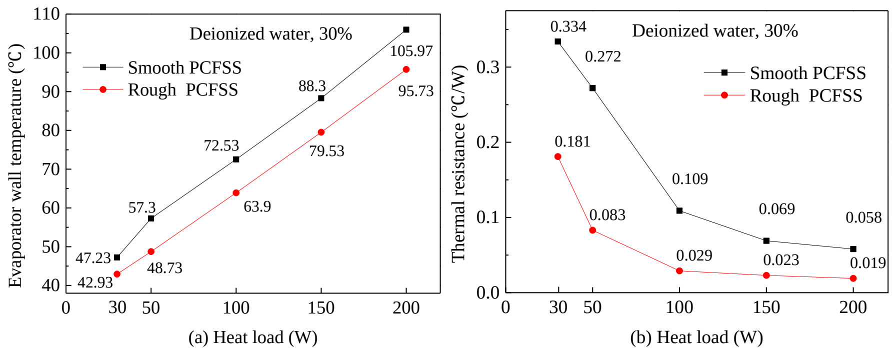

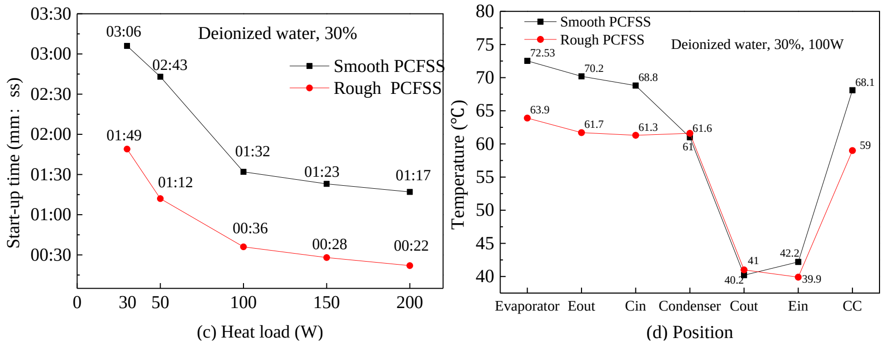

Fig. 10 Heat transfer characteristics of LHPs with rough and smooth PCFSSs under different heat load when deionized water with a 30% filling ratio was selected: (a) Evaporator wall temperature; (b) Thermal resistance; (c) Start-up time; (d) Temperature distribution along LHP. (Eout: evaporator outlet; Ein: evaporator inlet; Cout: condenser outlet; Cin: condenser inlet; CC: compensation chamber. The abbreviation similarly hereinafter.)

The surface morphology influenced the thermal performance of LHPs differently for a varied heat load, and the difference in the evaporator wall temperature increased and the difference in the thermal resistance decreased with increasing heat load, that is, the surface morphology had a greater influence on the thermal performance of LHPs at high heat load, as shown in Fig. 11. For example, the evaporator wall temperature difference was 4.3 °C with a heat load of 30 W; however, it increased to 10.22 °C when the heat load was increased to 200 W. In addition, the difference in thermal resistance decreased from 0.189 °C/W to 0.039 °C/W when the heat load was increased from 50 W to 200 W. The results can be attributed to the following: for a low heat load situation, the capillary force provided by rough and smooth wicks could drive the working fluid flow from the compensation chamber to the evaporation zone by a slow evaporation process. However, for a high heat load situation, the capillary force generated by the smooth wick was insufficient to provide enough liquid because the process whereby the working fluid evaporated was accelerated. The rough wick could provide a larger capillary force to maintain the cycle of working fluid in the LHP. In addition, the larger amount of liquid stored in the rough wick prevented the appearance of the dry-out phenomenon, resulting in a significant difference between the rough and smooth wicks at high heat load.

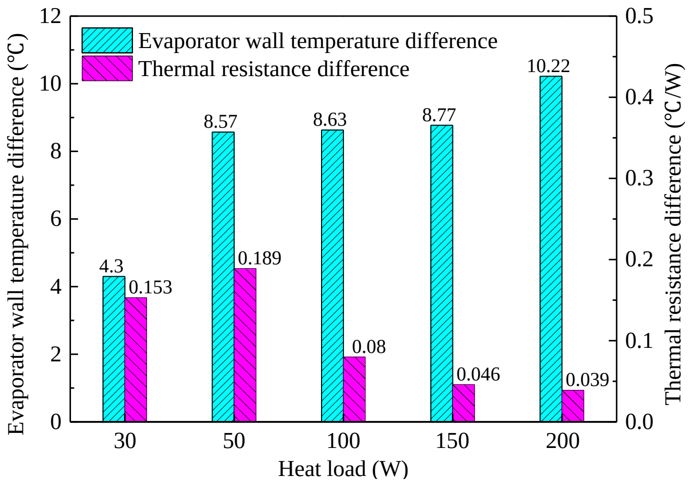

Fig. 11 Evaporator wall temperature and thermal resistance difference between smooth and rough PCFSSs with deionized water under different heat loads

Fig. 12 shows the thermal performance of LHPs with smooth and rough PCFSSs under different heat loads when ethanol with a 30 % filling ratio was used as working fluid. Similar to deionized water, the evaporator wall temperature, thermal resistance, and start-up time of LHPs with rough PCFSSs were all lower than those of the smooth PCFSSs. The evaporator wall temperature difference also tended to increase with increasing heat load, and the thermal resistance showed the opposite tendency. The temperature distribution near the evaporator with the rough PCFSS as wick was lower than that of the smooth PCFSS, and the temperature distribution near the condenser was exactly the opposite for a 100 W heat load.

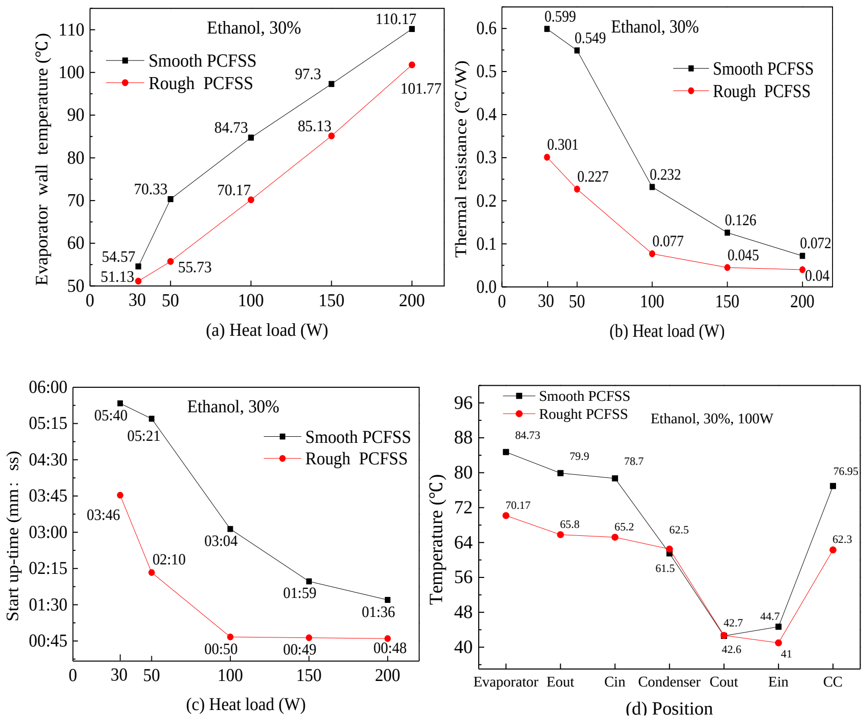

Fig. 12 Heat transfer characteristics of LHPs with rough and smooth PCFSSs under different heat load when ethanol with a 30% filling ratio was selected: (a) Evaporator wall temperature; (b) Thermal resistance; (c) Start-up time; (d) temperature distribution along LHP

Fig. 13 shows the thermal performance of LHPs with smooth and rough PCFSSs under different heat loads when acetone with a 30 % filling ratio was used as working fluid. The evaporator wall temperature, thermal resistance, start-up time, and temperature distribution along the loop of LHPs with smooth and rough PCFSSs changed slightly, as shown in Fig. 13. This could be due to the fact that acetone had excellent compatibility and wettability with copper fibers and copper tubes, as verified by the capillary pumping test in which acetone exhibited the fastest capillary pumping rate. The acetone steam flowed into the steam grooves, before easily transferring to the condenser, and readily producing a circular flow with a smaller driving force due to the smaller viscous limits [34]. Both the smooth PCFSS and rough PCFSS could provide the required driving force. Thus, the evaporator wall temperature, thermal resistance, and start-up time of LHPs with smooth and rough PCFSSs were all lower than 100 °C, 0.04 °C/W, and 20 seconds, respectively, for a heat load of 200 W.

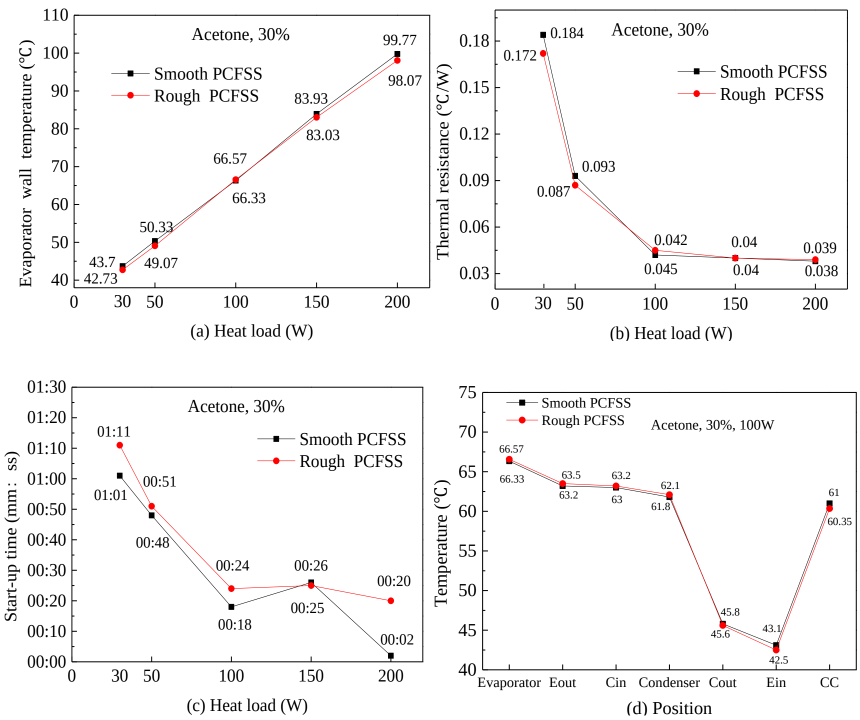

Fig. 13 Heat transfer performance of LHPs with rough and smooth PCFSSs under different heat load when acetone with a 30% filling ratio was selected: (a) Evaporator wall temperature; (b) Thermal resistance; (c) Start-up time; (d) Temperature distribution along LHP

3.2.2 Filling ratio

The filling ratio describes the volume of working fluid as a percentage of the total internal volume of an LHP. The appropriate filling ratio supplements the working fluid consumed in the evaporation process and provides sufficient space for steam transfer. In this study, the total internal volume of the LHP was approximately 67 cm^3 and the internal volume of the evaporator was approximately 25 cm^3. The filling ratio is calculated by following formula:

$$FR = \frac{V_l}{V_{total}} \times 100\% \qquad (19)$$

where FR is the filling ratio, V_l is the volume of liquid, V_{total} is the total internal volume of the LHP, and it contains:

$$V_{total} = V_w \varepsilon + V_{groove} + V_{s.line} + V_{cond} + V_{l.line} + V_{cc} \qquad (20)$$

where V_w, V_{groove}, $V_{s.line}$, V_{cond}, $V_{l.line}$, and V_{cc} represent the volume of the wick, steam grooves, steam line, condenser, liquid line, and compensation chamber, respectively, and ε is the porosity of the wick. Owing to the influence of gravity, the heat transfer performance of LHPs should consider the minimum filled-liquid volume limit. The filled-liquid mass limit in the wick is deduced as follows [35]:

$$Q_{FL,w} = \left(\frac{m_l}{xL_w} \right)^3 \frac{gh_{fg}}{3\pi^2 \mu_l \rho_l D_w{}^2 N^2} \qquad (21)$$

where $Q_{FL,w}$ is the filled-liquid mass limit of the wick, m_l is the mass of the liquid, and x is a constant coefficient, which was selected as 0.8 and 1 with and without the wick structure, respectively. Further, h_{fg}, μ, and ρ are the latent heat, dynamic viscosity, and density of the liquid, respectively, L_w and D_w are the length and equivalent diameter of the wick, respectively, and N is the number of wicks. The filled-liquid volume limit is derived by the following volume-quality relationship:

$$V_{FL,w} = \frac{Q_{FL,w}}{\rho_l} = \left(\frac{m_l}{xL_w} \right)^3 \frac{gh_{fg}}{3\pi^2 \mu_l \rho_l{}^2 D_w{}^2 N^2} \qquad (22)$$

This formula is appropriate to other parts of LHPs such as the liquid-steam line, condenser, compensation chamber, and steam grooves. It replaces the parameters L_w and D_w with those that are associated with the other parts of LHPs. The minimum filled-liquid volume limits of the parts listed above represents the filled-liquid volume limit of the LHP:

$$V_{FL,LHP} = \min(V_{FL,w}, V_{FL,groove}, V_{FL,s.line}, V_{FL,l.line}, V_{FL,cond}, V_{FL,cc}) \quad (23)$$

In this study, 15 %, 30 %, and 45 % filling ratios of deionized water were selected to study the influence of the filling ratio on the heat transfer performance of LHPs. Rough PCFSS was selected as the wick for its superior performance in both the capillary pumping and heat transfer performance tests. Fig. 14 shows the heat transfer performance of LHPs with deionized water as working fluid for different filling ratios. Selection of a 30 % filling ratio resulted in the minimum evaporator wall temperature and thermal resistance being observed for the LHPs. For a 15 % filling ratio, the evaporator wall temperature significantly increased with increasing heat loads. In particular, a lower evaporator wall temperature was obtained with a low heat load (30 W or 50 W). However, the evaporator wall temperature increased considerably with a high heat load, and exceeded 110 °C with a 200 W heat load. A 45 % filling ratio produced an evaporator wall temperature that was slightly higher than that of the 15 % filling ratio at low heat loads (less than 100 W). Conversely, the evaporator wall temperature increased slowly with high heat loads (more than 100 W), which was lower than that of the 15 % filling ratio. Therefore, when a 30 % filling ratio was selected, the LHP exhibited improved heat transfer performance in the heat load range of 30 - 200 W, which was consistent with the theoretical filling ratio of LHPs [22]. This was attributed to the fact that the reasonable filling ratio of the working fluid provided sufficient liquid working fluid for the evaporating process and enough space for the steam cycle such that a lower evaporator wall temperature and thermal resistance of LHPs could be obtained. For example, for a heat load of 100 W, the temperature distribution near the evaporator with a 30% filling ratio was lower than that of the 15% filling ratio, and it was exactly the opposite near the condenser; yet, the temperature distribution with a 45% filling ratio was the highest along the entire loop, indicating worse thermal performance, as shown in Fig. 14. (d). However, the start-up time of the LHP was a different situation. For a low heat load, the 15 % filling ratio exhibited the shortest start-up time, followed by the 30 % and 45 % filling ratios, respectively. For a high heat load, the start-up time varied little with different filling ratios. This could be attributed to the dependence of the start-up time on the time at which the evaporation occurred and transferred to the condenser. For a low heat load, the liquid was heated and reached its boiling point quickly with a lower filling ratio; conversely, when the filling ratio was high, much time was required to heat the liquid owing to the large amount of liquid stored in the compensation chamber and evaporation zone. Thus, the start-up time of the LHP was shortened as the filling ratio decreased from 45 % to 15 %. However, at high heat load, the heat flux was sufficiently large to heat the liquid stored in the evaporator in a short time, which reduced the time difference between the low and high filling ratios significantly.

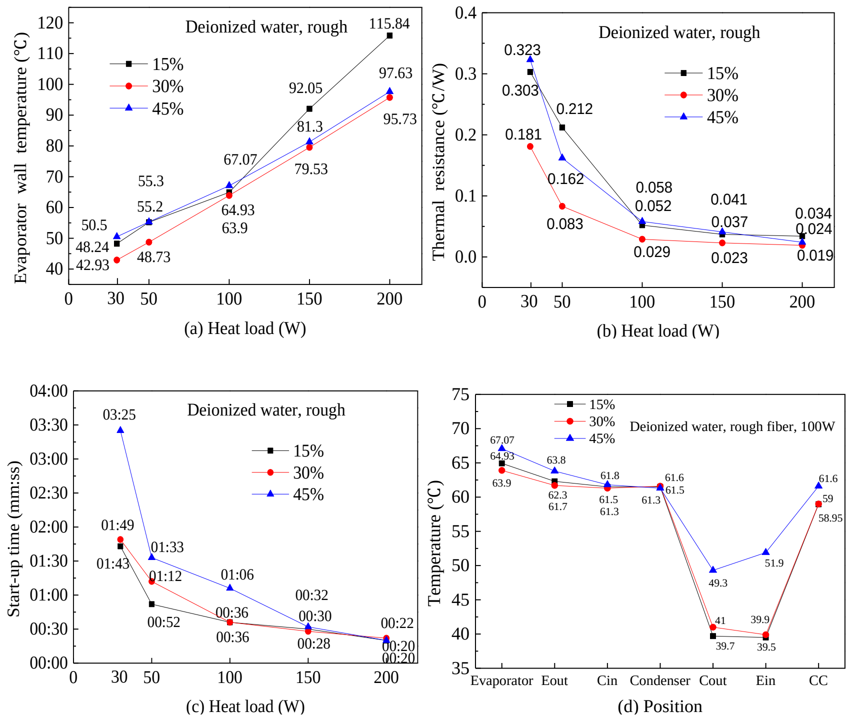

Fig. 14 Evaporator wall temperature and thermal resistance of LHPs under different heat loads with deionized water of different filling ratios: (a) Evaporator wall temperature; (b) Thermal resistance; (c) Start-up time; (d) Temperature distribution along LHP

3.2.3 Working fluid

Fig. 15 shows the thermal performance of LHPs with different working fluids. Rough PCFSS wicks and a 30% filling ratio were selected. With deionized water and ethanol as working fluids, the minimum and maximum evaporator wall temperatures and thermal resistances of LHPs were obtained, respectively. The shortest start-up time of the LHP was obtained when acetone was selected as the working fluid. This was attributed to the following: compared to the other two working fluids, deionized water has the largest latent heat and absorbed more heat to produce the lowest evaporator wall temperature. When the same volume of steam was transferred, the deionized water carried more heat into the condenser, thus resulting in a much lower evaporator wall temperature and lower thermal resistance of the LHPs. However, when acetone was used as the working fluid, it easily boiled in the evaporator and rapidly absorbed heat because it has the lowest boiling point, resulting in superior thermal performance relative to that of ethanol. As a result, the temperature distribution near the evaporator was the lowest with deionized water as the working fluid, and it was the highest with acetone as the working fluid when a 100 W heat load was selected, as shown in Fig. 15. (d). Furthermore, the start-up time of the LHP was the shortest with acetone as working fluid because of the fast evaporation process and excellent compatibility and wettability with copper material, as shown in Fig. 15 (c). The evaporator wall temperature and thermal resistance of LHP agreed well with the capillary pumping test results when deionized water, acetone, and ethanol were selected as working fluids.

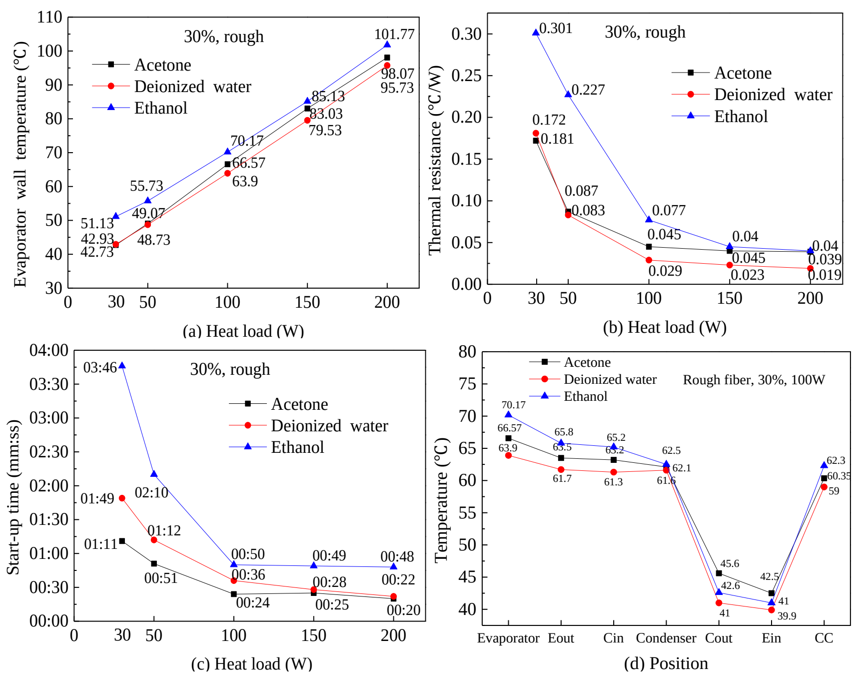

Fig. 15 Heat transfer performance of LHPs with different working fluids: (a) Evaporator wall temperature; (b) Thermal resistance; (c) Start-up time; (d) temperature distribution along LHP

3.3 Stable operation test

Fig. 16 shows the temperature curves of the LHP as a function of time at different testing points when rough PCFSS with a 70 % porosity and deionized water with a 30 % filling ratio were selected. The testing time was approximately 5.5 h. The temperature fluctuations of the LHPs were found to be negligible when the LHPs entered the stable operation stage after approximately 20 min. In this operation stage, the maximum and minimum evaporator wall temperatures were 97 °C and 94.9 °C, respectively. Thus, the temperature difference was about 2.1 °C with a standard deviation of 0.44. It was concluded that the wall temperature of the stable evaporator was controlled below 100 °C for a heat load of 200 W when the rough PCFSS wick was used for the LHP.

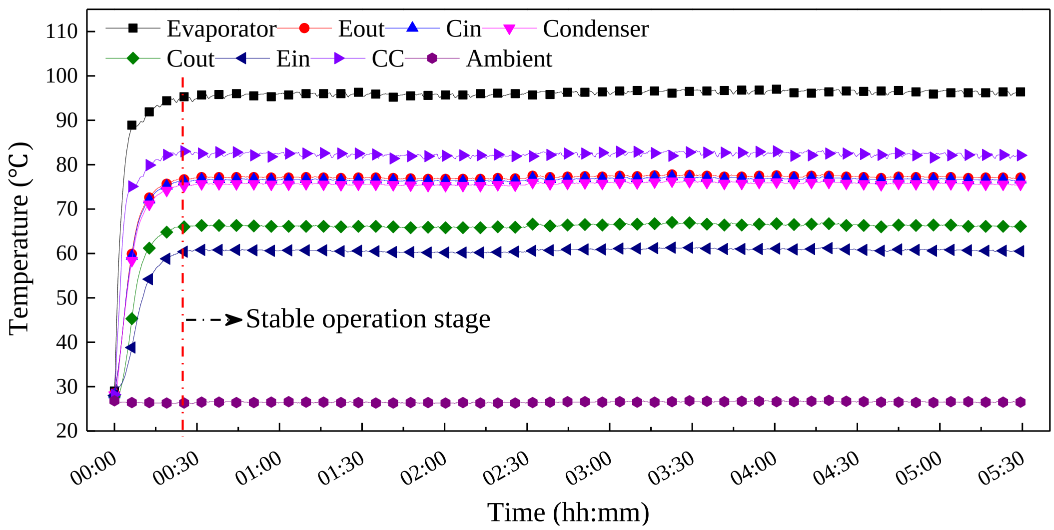

Fig. 16 Temperature curves of LHP over time at different testing point (Eout: evaporator outlet; Ein: evaporator inlet; Cout: condenser outlet; Cin: condenser inlet; CC: compensation chamber)

4 Conclusions

Rough copper fibers obtained by the multi-tooth tool cutting method and commercial smooth copper fiber obtained by the drawing method were selected to fabricate smooth and rough PCFSSs using a low-temperature solid-phase sintering method. A theoretical formula to calculate the capillary pumping amount and capillary pumping rate of PCFSSs was derived according to Darcy's law. The capillary pumping performance of the PCFSSs was then assessed to investigate the effects of the fiber surface morphology and working fluid on the capillary pumping performance. The experimental results obtained for the capillary pumping amount and capillary pumping rate agreed well with the theoretical results. Subsequently, the PCFSSs with smooth and rough surface morphologies were selected as wicks for LHPs. The thermal performance of the LHPs was assessed and the influence of the surface morphology, filling ratio, and working fluid on the evaporator wall temperature, thermal resistance, and start-up time of the LHPs was investigated in detail. The surface morphologies of the PCFSSs were found to greatly influence the thermal performance of the LHPs with different heat loads and working fluids. Finally, the optimal operation parameters of the LHPs were obtained. The main conclusions are listed as follows:

（1）Compared to smooth PCFSS, a larger capillary pumping amount and capillary pumping rate was observed for rough PCFSS. When deionized water, acetone, and ethanol were selected as working fluids, rough PCFSS with deionized water required the shortest time to stabilize and resulted in the maximum capillary pumping amount. Rough PCFSS exhibited the highest capillary pumping rate with acetone as working fluid.

（2）Compared with smooth PCFSS, much lower thermal resistance, evaporator wall temperature, and start-up time were obtained for LHPs with rough PCFSS when deionized water and ethanol were selected as working fluids. The surface morphology of PCFSS had little effect on the heat transfer performance of LHPs when acetone was selected as the working fluid.

（3）In the heat load range of 30–200 W, LHPs with a 30 % filling ratio exhibited enhanced heat transfer performance. The start-up time decreased with decreasing filling ratio for a low heat load, whereas the difference was insignificant for a high heat load.

（4）The minimum and maximum thermal performance of LHPs was obtained with deionized water and ethanol as working fluids, respectively, and the shortest start-up time was obtained when acetone was selected as the working fluid.

（5）With a 200 W heat load, LHPs with rough PCFSS exhibited improved performance and operated stably for a long time with little temperature fluctuation when a 30 % filling ratio was selected for deionized water as working fluid.

Acknowledgements

This work was supported by the Guangdong Natural Science Funds for Distinguished Young Scholars (No. 2016A030306032), Foundation of Public Welfare Research and Capacity Building in Guangdong Province (No.2014A010106002). The supports from the Fundamental Research Funds for Central Universities, Xiamen University (No. 20720160079), and the Collaborative Innovation Center of High-End Equipment Manufacturing in FuJian are also acknowledged.

References

[1] Yu YFM, Gerasimov F, Shchegolev GT, Filippov GA, Starikov LG, Kiseev VM, Dolgirev YE. Low-temperature heat pipes with separate channels for vapor and liquid. J Eng Physics and Thermophysics 1975; 28:683-5.

[2] Chen SJ, Yang J. Loop thermosyphon performance study for solar cells cooling. Energy Convers and Manage 2016; 121:297-304.

[3] Genk E, Mohamed S. Space nuclear reactor power system concepts with static and dynamic energy conversion. Energy Convers and Manage 2008; 49:402-11.

[4] Liu J, Pei NQ, Guo KH, He ZH, Li TX, Lv M. Experimental investigation on mechanical pumped cooling loop for application in future space missions. Energy Convers and Manage 2008; 49:2704-10.

[5] Ziapour BM, Kheljan, NY, Khalili MB. Performance study of solar water heater comprised of the separate loops flow boiling in the mini tubes. Energy Convers and Manage 2016; 111:245-52.

[6] Guo YD, Lin GP, Bai LZ, Bu XQ, Zhang HX, He J. Experimental study on the supercritical startup of cryogenic loop heat pipes with redundancy design. Energy Convers and Manage 2016; 118:353-63.

[7] Zhang XX, Shen JC, He W, Xu P, Zhao XD, Tan JY. Comparative study of a novel liquid-vapour separator incorporated gravitational loop heat pipe against the conventional gravitational straight and loop heat pipes - Part II: Experimental testing and simulation model validation. Energy Convers and Manage 2015; 93:228-38.

[8] Zhang XX, Shen JC, He W, Xu P, Zhao XD, Tan JY. Comparative study of a novel liquid-vapour separator incorporated gravitational loop heat pipe against the conventional gravitational straight and loop heat pipes - Part I: Conceptual development and theoretical analyses. Energy Convers and Manage 2015; 90:409-26.

[9] Tang Y, Deng DX, Lu LS, Pan MQ, Wang QH. Experimental investigation on capillary force of composite wick structure by IR thermal imaging camera. Exp Therm Fluid Si 2010; 34:190-6.

[10] Deng DX, Liang DJ, Tang Y, Peng JM, Han XD, Pan MQ. Evaluation of capillary performance of sintered porous wicks for loop heat pipe. Exp Therm Fluid Si 2013; 50:1-9.

[11] Boubaker R, Platel V. Vapor pocket behavior inside the porous wick of a capillary pumped loop for terrestrial application. Appl Therm Eng 2015; 84:420-8.

[12] Do KH, Kim SJ, Garimella SV. A mathematical model for analyzing the thermal characteristics of a flat micro heat pipe with a grooved wick. Int J Heat Mass Tran 2008; 51:4637-50.

[13] Wang YW, Cen JW, Jiang FM, Cao WJ, Guo J. LHP heat transfer performance: A comparison study about sintered copper powder wick and copper mesh wick. Appl Therm Eng 2016; 92:104-10.

[14] Choi J, Sano W, Zhang WJ, Yuan Y, Lee Y, Borca-Tasciuc DA. Experimental investigation on sintered porous wicks for miniature loop heat pipe applications. Exp Therm Fluid Si 2013; 51:271-8.

[15] Wu SC, Wang D, Lin WJ, Chen YM. Investigating the effect of powder-mixing parameter in biporous wick manufacturing on enhancement of loop heat pipe performance. Int J Heat Mass Tran 2015; 89:460-7.

[16] Zhang C, Xin GM, Wang H, Cheng L. Analysis of sintering parameters' influences on porous wicks for LHP. Energy Education Science and Technology Part A: Energy Science and Research 2014; 32:4737-44.

[17] Li H, Wang XG, Liu ZS, Tang Y, Yuan W, Zhou R, Li YJ. Experimental investigation on the sintered wick of the anti-gravity loop-shaped heat pipe. Exp Therm Fluid Si 2015; 68:689-96.

[18] Byon C, Kim SJ. Capillary performance of bi-porous sintered metal wicks. Int J Heat Mass Tran 2012; 55:4096-103.

[19] Chen BB, Liu W, Liu ZC, Li H,Yang JG. Experimental investigation of loop heat pipe with flat evaporator using biporous wick. Appl Therm Eng 2012; 42:34-40.

[20] Li H, Liu ZC, Chen BB, Liu W, Li C, Yang JG. Development of biporous wicks for flat-plate loop heat pipe. Exp Therm Fluid Si 2012; 37:91-7.

[21] Zhou W, Ling WS, Duan L, Hui KS, Hui KN. Development and tests of loop heat pipe with multi-layer metal foams as wick structure. Appl Therm Eng 2016; 94:324-30.

[22] Ling WS, Zhou W, Liu RL, Qiu QF, Liu J. Thermal performance of loop heat pipe with porous copper fiber sintered sheet as wick structure. Appl Therm Eng 2016; 108: 251–260.

[23] Nishikawara M, Nagano H. Numerical simulation of capillary evaporator with microgap in a loop heat pipe. Int J Therm Sci 2016; 102:39-46.

[24] Liu ZC, Wang DD, Jiang C, Yang JG, Liu W. Experimental study on loop heat pipe with two-wick flat evaporator. Int J Therm Sci 2015; 94:9-17.

[25] Li JW, Zou Y, Cheng L. Experimental study on capillary pumping performance of porous wicks for loop heat pipe. Exp Therm Fluid Si 2010; 34:1403-8.

[26] Zhou W, Wang QH, Li JR, Tang Y, Huang ZM, Zhang JP. Hydrogen production from methanol steam reforming using porous copper fiber sintered felt with gradient porosity. Int J Hydrogen Energ 2015; 40:244-55.

[27] Liu RL, Zhou W, Ling WS, Xiang JH, Chen KJ. Fabrication of continuous slim aluminum fibers using a multi-tooth tool. Mater Manuf Process 2016:1-7.

[28] Tharayil T, Asirvatham LG, Ravindran V, Wongwises S. Effect of filling ratio on the performance of a novel miniature loop heat pipe having different diameter transport lines. Appl Therm Eng 2016; 106:588-600.

[29] Nakamura K, Odagiri K, Nagano H. Study on a loop heat pipe for a long-distance heat transport under anti-gravity condition. Appl Therm Eng 2016; 107:167-74.

[30] Huang X, Wang QH, Zhou W, Deng DX, Zhao YW, Wen DH, Li JR. Morphology and transport properties of fibrous porous media. Powder Technol 2015; 283:618-26.

[31] Taylor JR, An Introduction to Error Analysis, 2nd ed, University Science Book, US, 1997.

[32] Tang Y, Deng DX, Huang GH, Wan ZP, Lu LS, Effect of fabrication parameters on capillary performance of composite wicks for two-phase heat transfer devices. Energy Convers and Manage, 2013; 66: 66-76.

[33] Wu R, Kharaghani A, Tsotsas E. Two-phase flow with capillary valve effect in porous media. Chem Eng Sci 2016; 139:241-8.

[34] Li Q, Zhao K, Xuan YM. Simulation of flow and heat transfer with evaporation in a porous wick of a CPL evaporator on pore scale by lattice Boltzmann method. Int J Heat Mass Tran 2011; 54:2890-901.

[35] Wang ZY, Zhao XD. Analytical study of the heat transfer limits of a novel loop heat pipe system. Int J Energ Res 2011; 35:404-14.